Chinese Journal of
POLYMER SCIENCE

RESEARCH ARTICLE

https://doi.org/10.1007/s10118-023-3023-2
Chinese J. Polym. Sci. **2024**, *42*, 352–363

Understanding the Thermal Impedance of Silicone Rubber/Hexagonal Boron Nitride Composites as Thermal Interface Materials

Yuan Ji[a], Shi-Da Han[a], Hong Wu[a*], Shao-Yun Guo[a], Feng-Shun Zhang[b], and Jian-Hui Qiu[c]

[a] *The State Key Laboratory of Polymer Materials Engineering, Sichuan Provincial Engineering Laboratory of Plastic/Rubber Complex Processing Technology, Polymer Research Institute, Sichuan University, Chengdu 610065, China*
[b] *Institute of Chemical Materials, China Academy of Engineering Physics, Mianyang 621900, China*
[c] *Department of Mechanical Engineering, Faculty of Systems Science and Technology, Akita Prefectural University, Akita 015-0055, Japan*

Abstract Silicone rubber (SR) composites are most widely used as thermal interface materials (TIMs) for electronics heat dissipation. Thermal impedance as the main bottleneck limiting the performance of TIMs is usually neglected. Herein, the thermal impedance of SR composites loaded with different levels of hexagonal boron nitride (h-BN) as TIMs was elaborated for the first time by the ASTM D 5470 standard test and finite element analysis. It was found that elastic modulus and surface roughness of SR composites increased with the increase of h-BN content, indicating that the conformity was reduced. When the assembly pressure was 0.69 MPa, there existed an optimal h-BN content at which the contact resistance was minimum (0.39 $K{\cdot}cm^2{\cdot}W^{-1}$). Although the decreased bond line thickness (BLT) by increasing the assembly pressure was beneficial to reduce the thermal impedance, the proper assembly pressure should be selected to prevent the warpage of the contact surfaces and the increase in contact resistance, according to the compression properties of the SR composites. This study provides valuable insights into fabrication of high-performance TIMs for modern electronic device applications.

Keywords Thermal interface materials; Hexagonal boron nitride; Thermal impedance; Surfaces

Citation: Ji, Y.; Han, S. D.; Wu, H.; Guo, S. Y.; Zhang, F. S.; Qiu, J. H. Understanding the thermal impedance of silicone rubber/hexagonal boron nitride composites as thermal interface materials. *Chinese J. Polym. Sci.* **2024**, *42*, 352–363.

INTRODUCTION

Modern electronic devices are rapidly developing toward miniaturization and high-power integration.[1–4] Efficient heat dissipation has become a prerequisite for reliable operation in electronic devices including computers, power batteries and 5G communications.[5–7] Otherwise, the large amount of accumulated heat could lead to equipment damage or even endanger human safety. Thermal interface materials (TIMs) based on polymer composites, which are most widely used for enhancing heat dissipation inside various devices, are placed between the interfaces of two components (such as processors and heat sinks) to improve the thermal transfer between them.[8,9] Silicone rubber (SR) has been used as the dominant matrix for TIMs due to its flexibility, high thermal stability and electrical insulation properties.[10–14] However, the low thermal conductivity value of SR is not directly applicable to heat dissipa- tion.[15,16] Therefore, incorporating various fillers into SR to construct thermally conductive networks is a general method to increase the thermal conductivity of SR composites as TIMs.[17,18]

Actually, excellent electrical insulation performance of TIMs is also desired in many application occasions such as transformers and power batteries, *etc*.[19,20] Among the numerous fillers, hexagonal boron nitride (h-BN) is a very promising one because of high electrically insulating and thermally conductive properties as well as oxidation resistance.[21–24] Several studies have verified that thermal conductivity can be significantly enhanced when the h-BN loading reaches the percolation threshold for thermally conductive networks in SR composites.[25–27] Gu *et al*. reported that a high thermal conductivity value of 1.11 $W{\cdot}m^{-1}{\cdot}K^{-1}$ was achieved in SR composites with a volume fraction of 40 vol% of h-BN filler, which was six times higher than that of pure SR.[28] Sebnem *et al*. also reported that flake-like h-BN with a high aspect ratio was more conducive to improving the thermal conductivity of SR composites than other shapes.[29] Although the massive loading of h-BN improves the thermal conductivity of the composites, mechanical properties such as flexibility,[30,31] elasticity[11] and hardness[10] are also sacrificed. Moreover, the reduced flexibility of the SR composites results in the inability of the SR composites to fill the interfacial voids completely, which affects the thermal conductance at the interfaces.[32,33] Consequently, the high thermal conductivity of TIMs does not imply efficient heat dissipation.

TIMs are originally designed to reduce the thermal impedance at the interfaces between the heat-generating device and the heat sink, the thermal conductivity should not be the only criterion to evaluate the performance of TIMs.[1,33]

* Corresponding author, E-mail: wh@scu.edu.cn
Received May 29, 2023; Accepted June 27, 2023; Published online August 22, 2023

The thermal impedance consists of bulk resistance and contact resistance. The bulk resistance is the thermal resistance of the TIMs themselves by conduction and depends on the bond line thickness (BLT) and the thermal conductivity of the TIMs.[34] The contact resistance is the thermal resistance at the interfaces between the TIMs and heat sink as well as the electronic device.[35,36] Besides the thermal conductivity, the contact thermal resistance and BLT are also intimately related to the filler content, since they both depend on the mechanical response of the composites to the assembly pressure.[37,38] Up to now, how SR composites loaded with different levels of h-BN influence the contact resistance and the BLT is unclear. Therefore, understanding the thermal impedance of SR composites as TIMs is of great significance for fabricating high-performance TIMs.

In this work, the effect of the morphological structure of SR composites loaded with different levels of h-BN on the thermal conductivity and mechanical properties was investigated. Furthermore, ASTM D 5470 test was used to elaborate the thermal impedance of the SR composites as TIMs. Finite element analysis simulation was applied to better visualize the effect of thermal impedance on heat dissipation. The enhancement mechanism of thermal conductivity was revealed. The influence of h-BN loading level and assembly pressure on the thermal impedance of SR composites was discussed in detail.

EXPERIMENTAL

Materials

Methylvinyl silicone rubber (110-2, M_n=6.9×10^5) with 0.17 wt% vinyl content was provided by Dongjue Silicone Group Co., Ltd., China. Hexagonal boron nitride (20–25 μm) was supplied by Suzhou Nutpool Materials Technology Co., Ltd., China. The vulcanizator, 2,5-dimethyl-2, 5-di-(*tert*-butylperoxy) hexane (DBPMH) was purchased from Hunan Yixiang Technology Co., Ltd., China.

Preparation of Composites

Firstly, SR, DBPMH, h-BN and were mixed in a torque rheometer (MIX-200C, Harbin Harp Electrical Technology Co., Ltd., China) at 40 °C with a rotation rate of 60 r/min for 15 min. To avoid agglomeration of h-BN at high filling level, the h-BN was added in several times. The compounds where the mass ratio of SR to DBPMH was fixed at 100 to 1.5. h-BN loading level varied as 0, 30, 60, 90, 120, 150 and 180 parts per hundred grams of silicone rubber (phr), and the corresponding mass fractions are 0 wt%, 23.1 wt%, 37.5 wt%, 47.4 wt%, 54.5 wt%, 60 wt% and 64.3 wt%. The compounds were then vulcanized at 165 °C with 10 MPa pressure for 12 min in a mold frame of 2 mm thickness. The composites were named as SR*x*, where *x* was added phr of the h-BN. For instance, the sample designation SR90 represents the composites filled with 90 phr (47.4 wt%) h-BN particles.

Characterization

Dispersion and orientation of fillers were analyzed by scanning electron microscopy (SEM, JSM-5900LV, Japan). The surface roughness of the composites was characterized by 3D profiler (KEYENCET, VR6200, Japan). The degree of filler orientation was measured by X-ray diffraction (XRD, Ultima IV, Japan) in a 2θ range from 10° to 80° at a scan rate of 0.06 (°)·s^{-1}, employing Cu Kα radiation. The rheological properties of samples were scanned from high to low frequencies (50–0.05 Hz) using a rotational rheometer (AR1500EX, USA) at 40 °C with a strain of 1% (within the linear viscoelastic region). The density of samples was tested by a densitometer (GH-120M, Matsuhaku, China). The hardness of samples was measured by Shore A hardness tester (LAC-YJ, Shandong Zhongke Puri Testing Technology Co., Ltd., China). The tensile properties of the samples were measured by a universal testing machine (CMT-4104, SANS, China) with a tensile rate of 200 mm/min at room temperature. The compression performance of the composites was tested by a dynamic mechanical analyzer (DMA, Q800, TA Instrument, USA) with a ramp force of 3.0 N/min to 15.0 N at room temperature.

The anisotropic thermal conductivity (λ) of samples was measured by a transient plane heat source method equipment (HotDisc1500, Sweden) at room temperature. In this work, the thermal impedance of SR composites was evaluated by a thermal interface materials tester under different pressures according to ASTM D 5470[39] (shown in Fig. 1a) manufactured by LINSEIS (Shanghai) Scientific and Instruments Co., Ltd. In detail, the sample was placed between two isothermal parallel metal blocks of uniform thickness, and the thermal gradient was applied to the specimen through the temperature difference between the two contacting surfaces, resulting in the heat flow through the specimen. The heat flow was perpendicular and uniform across the test surface, as there was no heat transfer laterally. The thermal impedance (θ) was calculated by the following equation:

$$\theta = \frac{A}{Q} \cdot (T_H - T_C) \quad (1)$$

where A is the area of specimen contact surfaces, Q is the heat flow rate between the two isothermal surfaces, T_H was the temperature of the hot meter bar, and T_C is the temperature of the cold meter bar. Contact resistance (R_c) is the intercept of the line, which was derived from fitting the measured θ at different BLTs.

The θ at the interface after inserting TIMs between the metal blocks has two components: the bulk resistance (R_{bulk}) arising from thermal conductivity, and contact resistance, R_c between the TIMs and the blocks as shown in Fig. 1(a). θ was given by:

$$\theta = R_{bulk} + R_{c1} + R_{c2} \quad (2)$$

The effective thermal conductivity (λ_{eff}) including contact resistance was calculated by the following equation:

$$\lambda_{eff} = \frac{BLT}{\theta} \quad (3)$$

Finite element analysis was used to investigate the heat dissipation process of the CPU cooling system, as shown in Fig. 1(b). The internal heat generation of the CPU was 2 W·cm^{-3}, and the convection coefficient of the aluminum heat sink was 0.005 W·cm^{-2}·°C^{-1}). The initial temperature of the CPU system was 25 °C, and the process of its temperature change was simulated by transient simulation.

RESULTS AND DISCUSSION

Morphologies of the Composites

The dispersion and orientation of h-BN in composites with different h-BN contents were observed by SEM, as shown in Fig. 2. There is no obvious agglomeration even when h-BN is filled up to 180 phr, due to multiple-addition of the h-BN. h-BN with low

https://doi.org/10.1007/s10118-023-3023-2

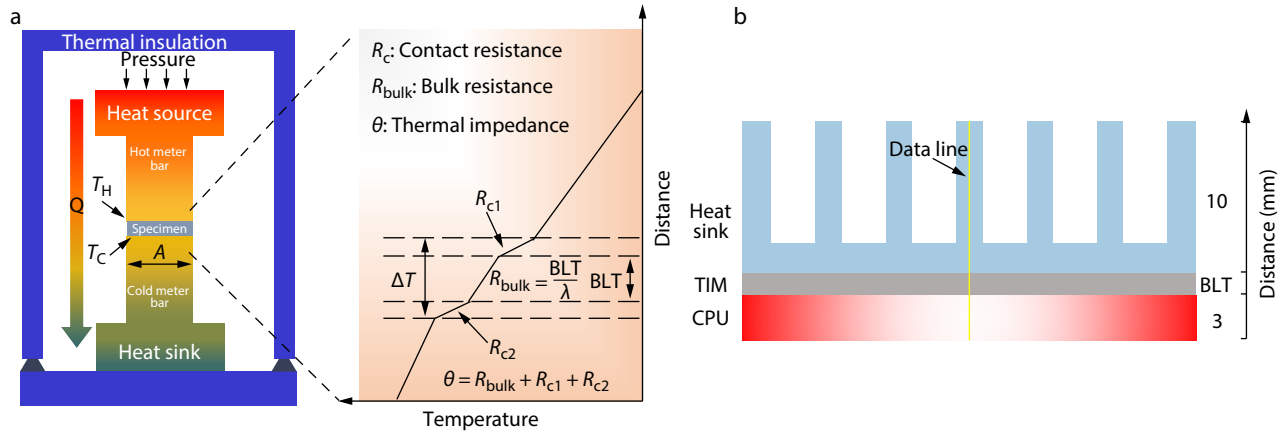

Fig. 1 (a) Schematics of the ASTM D 5470 test; (b) Demonstration of dissipation heat system of simulation with a CPU, TIM, and aluminum heat sink.

loadings exhibits random distribution in the SR matrix (Fig. 2a), and few contacts between h-BN flakes provide limited thermally conductive networks. As shown in Figs. 2(b) and 2(c), h-BN flakes are gradually aligned along the in-plane direction with increasing the h-BN content. This indicates that the thermally conductive networks, which benefits heat flow dissipation along the in-plane direction, are gradually formed.[40–42] It can be seen that the h-BN flakes are densely stacked and a more complete thermally conductive network is constructed when the h-BN loading reaches 120 phr.

The microstructure properties of the composites could be further analyzed by rheological testing. Fig. 3 demonstrates the complex viscosity, storage modulus and loss modulus versus the frequency of the composites at a strain value of 1%. The complex viscosity of the composites decreases significantly with increasing the frequency, exhibiting non-Newtonian behavior. As shown in Fig. 3(a), the complex viscosity of the composites in the low-frequency region is much higher than that of pure SR, when the introduction of h-BN is above 120 phr. It is ascribed that the friction between densely stacked h-BN flakes leads to huge energy dissipation. As for the storage modulus, a plateau forms in the low-frequency region when the h-BN content is greater than 120 phr, which is attributed to the thermally conductive network formed by h-BN hinders the continuous flow of SR molecular chains.[10] When the content of h-BN increased, the loss modulus of the composites increases while the slopes of curves decrease, indicating that the flow capacity of the composite is reduced (Fig. 3c). Although the high content of h-BN facilitates the construction of thermally conductive networks, the dramatic increase in the viscosity may limit the processing of the composites.[43]

Different top and side XRD diffraction patterns could be used to reveal the orientation of the h-BN. As shown in Fig. 4(a), three characteristic diffraction peaks near 26.8°, 41.6° and 55° correspond to (002), (100) and (004) crystallographic

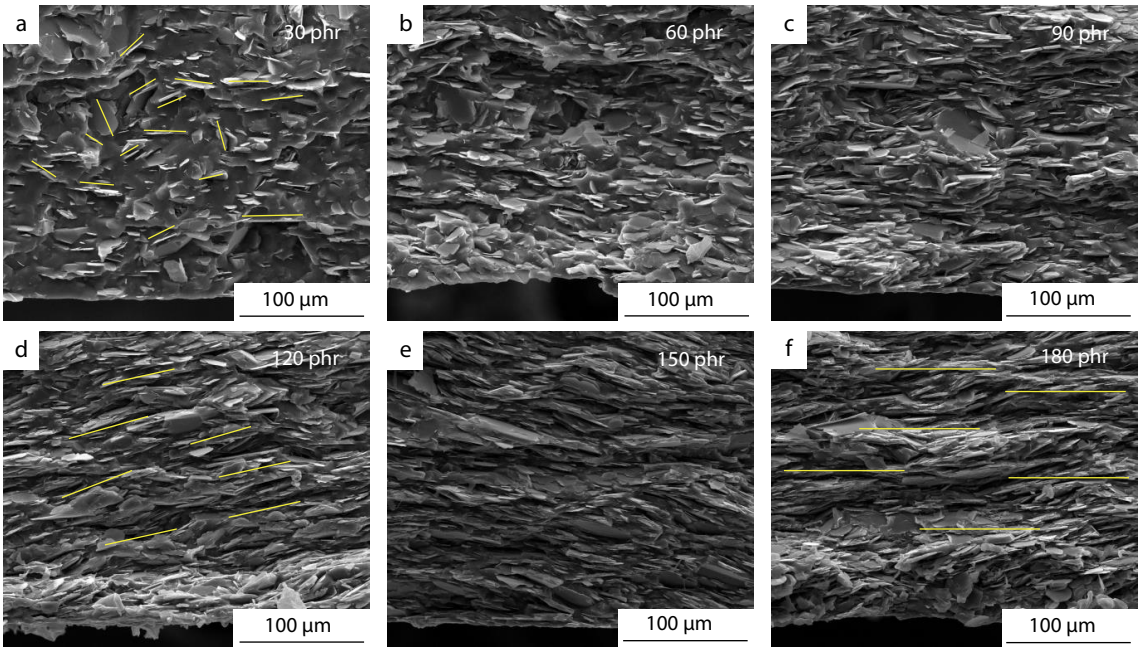

Fig. 2 Cross-sectional SEM images of the composites with different h-BN loadings (red bars mean the orientation direction of h-BN).

https://doi.org/10.1007/s10118-023-3023-2

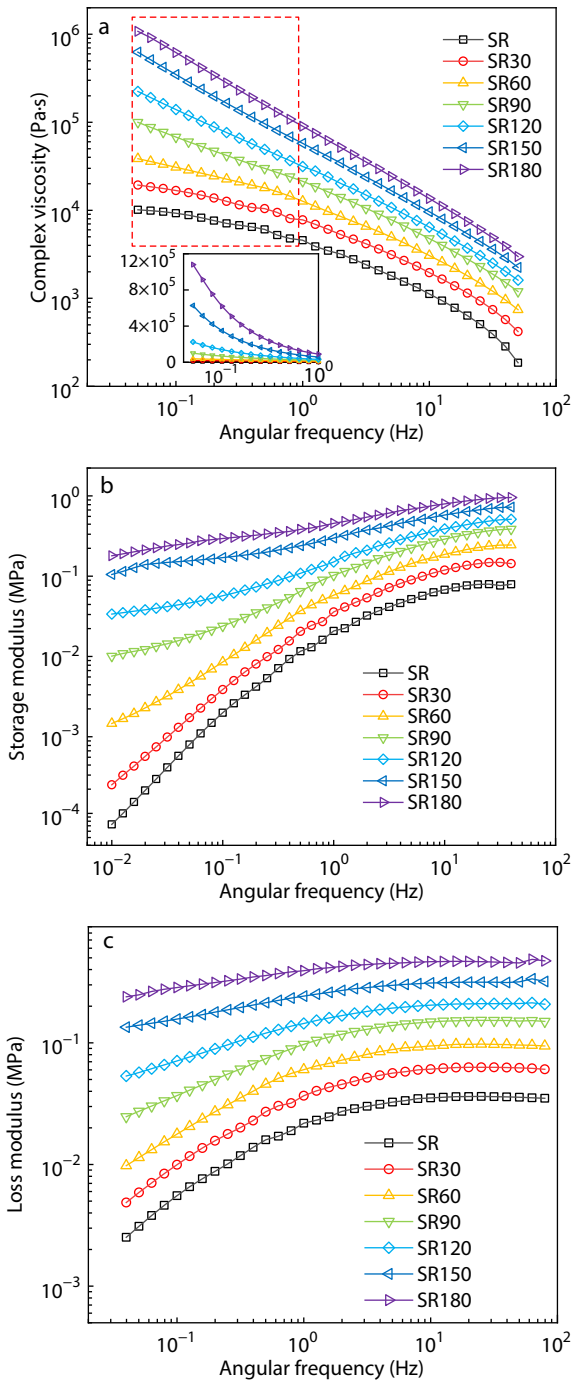

Fig. 3 Rheological properties of the composites: (a) complex viscosity, (b) storage modulus, (c) loss modulus.

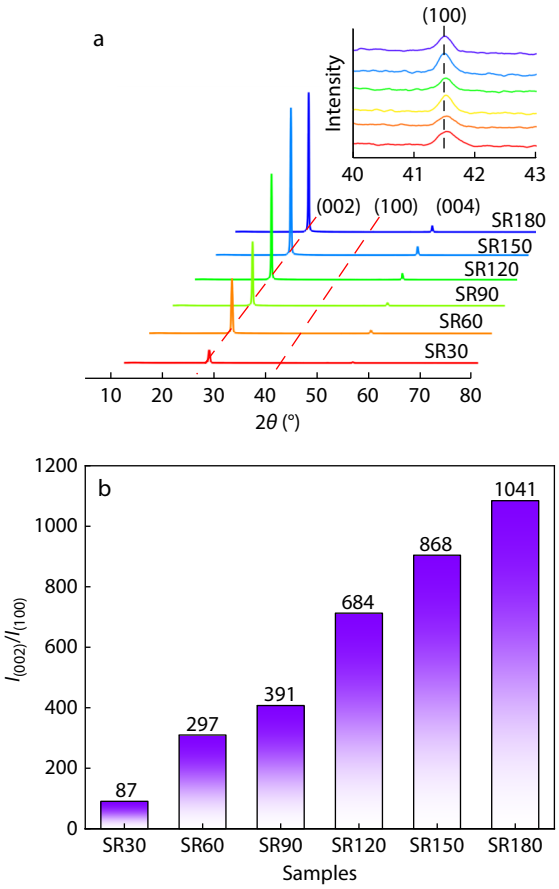

Fig. 4 (a) XRD patterns of the composites along the in-plane direction; (b) The intensity ratio of $I_{(002)}$ to $I_{(100)}$ with various h-BN contents.

planes of h-BN, respectively.[14,44,45] The diffraction of the (002) plane is parallel to the hexagonal plane of h-BN, *i.e.*, the peak intensity of (002) represents the horizontally aligned h-BN. If the h-BN alignment is along the in-plane direction, it will lead to an increase in the intensity of (002) and a decrease in the intensity of (100). Hence the larger intensity ratio of $I_{(002)}/I_{(100)}$ signifies better in-plane orientation of h-BN flakes. Fig. 4(b) shows that an increase in the loading of the h-BN causes a higher ratio of $I_{(002)}/I_{(100)}$, and the intensity ratio of SR180 is 10 times more than that of pure SR, indicating that a high loading level can benefit the in-plane orientation, which is consistent with SEM results.

Mechanical Properties of the Composites

The typical stress-strain curves of the SR composites with different h-BN contents are shown in Fig. 5(a). The tensile strength of pure SR is only 0.43 MPa, and the addition of h-BN increases the tensile strength of the composites (Fig. 5b). SR30 has a significantly superior elongation at break, since the stresses acting on the SR molecular chains are uniformly transferred by the h-BN flakes. When the h-BN content is further increased, the decrease in the crosslink point density of the SR matrix and the inevitable stress concentration due to interfacial defects, leading to a decrease in the elongation at break of the composites.[46] Fortunately, the elongation at break of the SR composite reaches 34.8% even with the incorporation of 180 phr h-BN due to the slippage of the orientated h-BN in the tensile (in-plane) direction.

For TIMs, the conformity refers to the replacement of air-filled microscopic voids by deformation at assembly pressure to reduce thermal interfacial resistance. All the composites exhibit compression elasticity deformation measured by a DMA instrument with a pressure of 15 N, as shown in Fig. 5(c). As the h-BN content increases from 0 phr to 180 phr, the compressive strain of the composites shows a non-linear decrease from 20.02% to 2.69%. This is attributed to the motion

https://doi.org/10.1007/s10118-023-3023-2

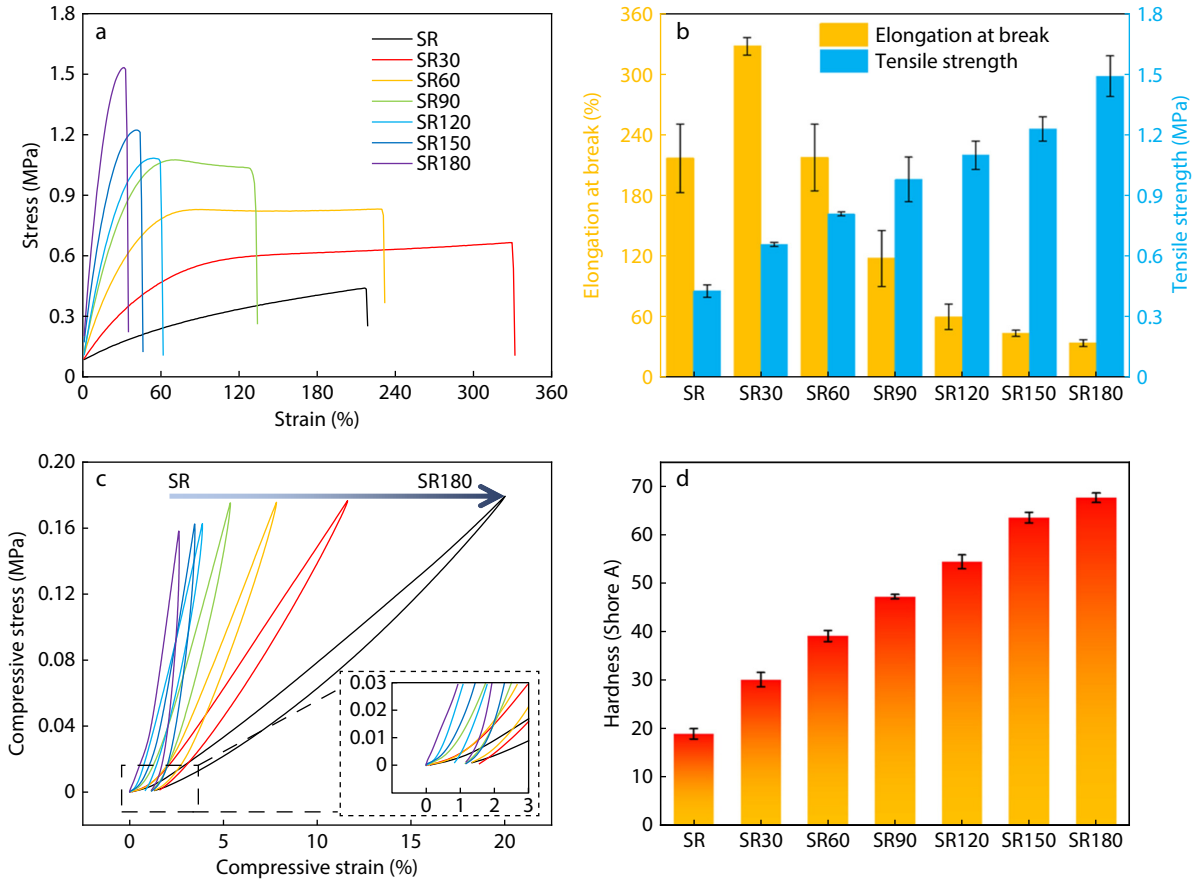

Fig. 5 Mechanical properties of SR composites: (a) tensile stress-strain curves, (b) elongation at break and tensile strength, (c) compressive stress-strain curves, and (d) hardness with different h-BN contents.

of SR molecular chains in the compression direction is limited by the dense stacking and in-plane orientation of h-BN.[47]

Table 1 shows the elastic modulus and deformation ratio of the composites with different h-BN contents (deformation ratio can be calculated by $(T_0 - T)/T_0$, where T_0 is the virgin thickness of the specimen before compression, and T is the thickness of the specimen after compression). It can be seen that the strain of all composites cannot be fully recovered to 0% after compression, resulting in permanent deformation. The composites present a much higher deformation ratio and show extremely poor elastic recover, with the increase of the h-BN content. The compression results show that the flexibility and elasticity of the SR composites are decreased distinctly, although the thermal conductivity increased with an increase of the h-BN content. Furthermore, the hardness of the composites with different h-BN content are shown in Fig. 5(d). The hardness of the composites increases rapidly from 19 shore A to 67.7 shore A with increasing the h-BN content, which means that the deformability of the composites is reduced. Consequently, high loading of the h-BN will hinder the conformity of the SR composites.

Thermal Transfer Performance of the Composites

The in-plane and through-plane thermal conductivity of the SR composites with different h-BN loadings were characterized. As shown in Fig. 6(a), the value of in-plane thermal conductivity ($\lambda_{\text{In-plane}}$) rapidly increases from 0.20 W·m^{-1}·K^{-1} to 7.04 W·m^{-1}·K^{-1} as the content of h-BN increases from 0 phr to 180 phr, while the value of through-plane thermal conductivity ($\lambda_{\text{Through-plane}}$) only increases to 1.01 W·m^{-1}·K^{-1}. It is ascribed that the thermally conductive networks constructed by the dense stacking and in-plane orientation of h-BN with increasing its content can transfer heat efficiently in the in-plane direction.[11,12,45]

To further elucidate the effect of orientation structure on the thermal conductivity of the composites, the anisotropy index (AI) is defined as:

$$\text{AI} = \frac{\lambda_{\text{In-plane}}}{\lambda_{\text{Through-plane}}} \times 100\% \quad (4)$$

where $\lambda_{\text{In-plane}}$ and $\lambda_{\text{Through-plane}}$ correspond to the thermal conductivity of the in-plane and through-plane, respectively. In Fig. 6(b), the AI increases almost linearly to over 700% with increasing the h-BN content, which means that $\lambda_{\text{In-plane}}$ increases remarkably faster than $\lambda_{\text{Through-plane}}$.

Fig. 6(c) illustrates the variation of the heat conduction mechanism of the composites with different loading levels of h-BN. The enhancement in the λ of the composites can be ascribed that the spatial confinement under hot-pressing results in the dense stacking and in-plane orientation of the h-BN. With the increase of the h-BN content, the degree of the orientation increases and thermally conductive networks are gradually formed. This will not only reduce contact thermal resistance between the h-BN flakes greatly but also induce the transfer of heat flow along the in-plane direction.[6,48]

https://doi.org/10.1007/s10118-023-3023-2

Table 1 The compressive strain, elastic modulus, and deformation ratio of the SR composites with different h-BN contents.

Sample	Strain at 15 N (%)	Elastic modulus (MPa)	Deformation ratio (%)
SR	20.02	0.90	5.9
SR30	11.61	1.52	13.9
SR60	7.92	2.20	17.2
SR90	5.37	3.26	19.7
SR120	3.88	4.17	22.4
SR150	3.47	4.55	33.4
SR180	2.69	5.57	44.3

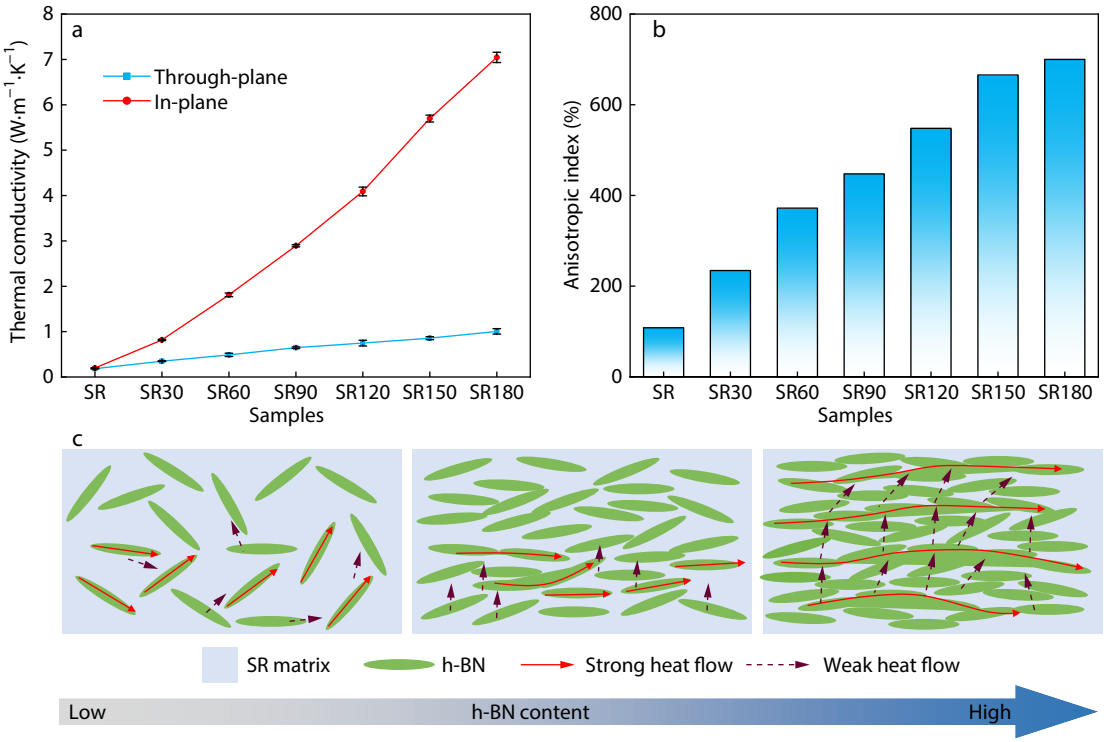

Fig. 6 (a) Thermal conductivity and (b) anisotropic index of the composites with different content of h-BN; (c) Diagram of heat conduction mechanism of the composites.

However, the heat flow cannot be transferred efficiently in the vertical direction because of the low thermal conductivity of h-BN in the transverse direction, even with the dense stacking of h-BN.[49] Therefore, the enhancement of $\lambda_{In\text{-}plane}$ is particularly significant with the increase of the h-BN content, as shown in Fig. 6(a).

Generally, the TIMs are used to reduce thermal interfacial resistance between the processor and the heat sink, thus the thermal impedance can more accurately reflect the thermal transfer performance of SR composites as TIMs.[3] As shown in Fig. 1(a), the thermal impedance of the composites was measured with a TIM testing system based on the ASTM D 5470 standard. Fig. 7(a) shows that the thermal impedance decreases dramatically when the filler content is within 90 phr, and then flattens out. The BLT is determined by the distance between the two copper blocks, where the composites are placed at a certain assembly pressure. The results are illustrated in Fig. 7(b) that BLT increases with increasing the h-BN content. The contact resistance is the intercept of the line, which is derived from fitting the measured thermal impedance at different BLTs. It is found that the thermal impedance increases significantly as the thickness gradually decreases (Fig. 7c). It can be seen in Fig. 7(d) that the contact resistance of the composites at an assembly pressure of 0.69 MPa decreases first and then increases with the increase of the h-BN content. The SR90 shows the minimum contact resistance with a value of 0.39 $K{\cdot}cm^2{\cdot}W^{-1}$.

In addition, the thermal impedance of the composites should be influenced by the assembly pressure, since it depends not only on the thermal conductivity but also on the mechanical response of the composites to pressure.[50] Fig. 7(e) shows a decrease in the thermal impedance of different composites at pressures from 0.069 MPa to 1.38 MPa. However, the λ_{eff} of all the composites increases first and then decreases with the increase of the assembly pressure, as demonstrated in Fig. 7(f). The obvious increase in λ_{eff} is attributed to removal from the interfacial air-filled voids. However, the reduction can be ascribed to the warpage of the contact surfaces under excessive assembly pressure, resulting in an increase in the contact resistance. Therefore, there exists an optimal pressure, since the λ_{eff} will decrease despite the further decrease of the thermal impedance.

To simulate the performance of the SR composite as TIMs, finite element analysis was used to investigate the heat dissi-

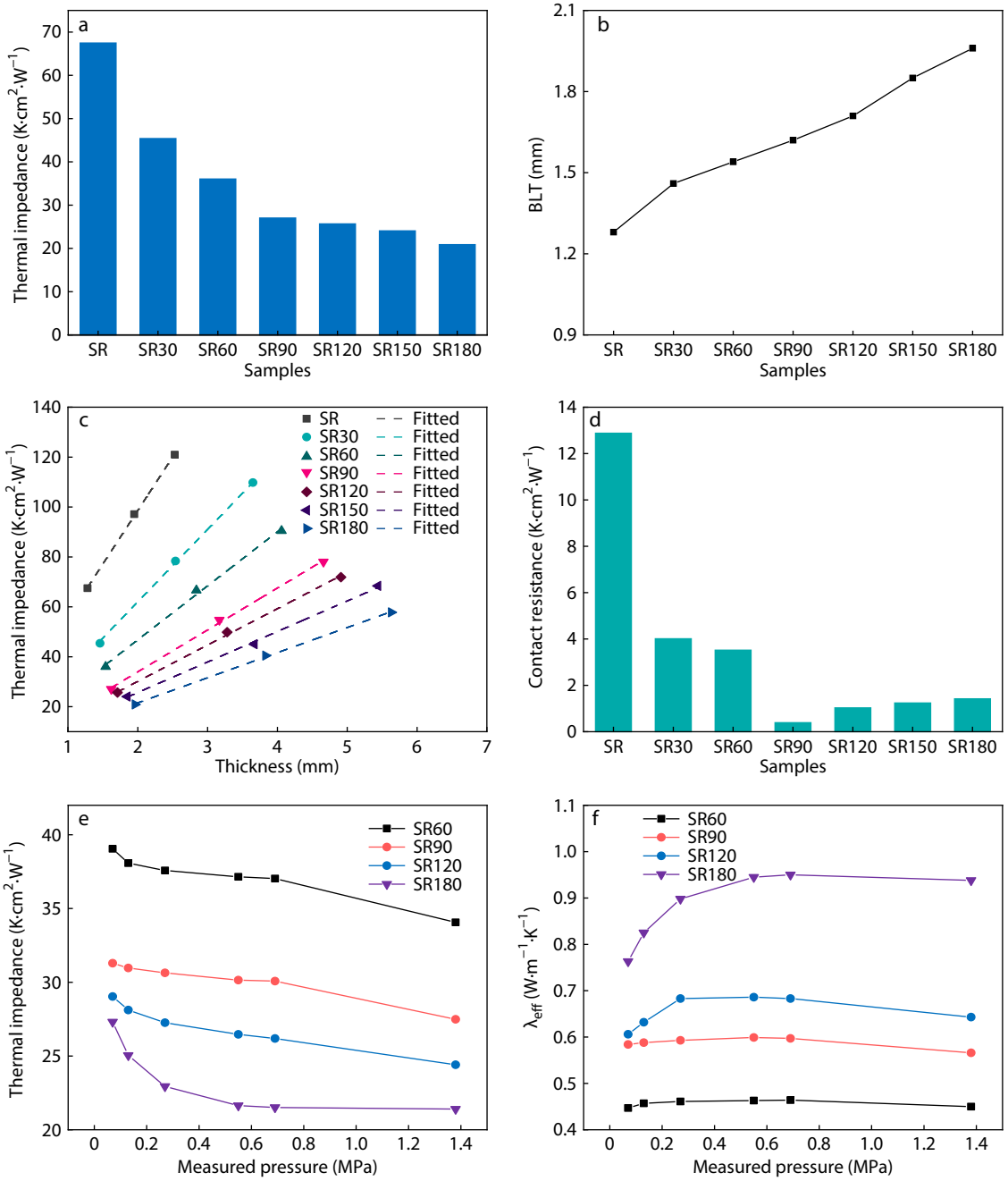

Fig. 7 (a) The thermal impedance and (b) BLT of the composites with different contents of h-BN at assembly pressure of 0.69 MPa; (c)The thermal impedance of the composites with varying thickness at assembly pressure of 0.69 MPa; (d) The contact resistance of composites with different contents of h-BN; (e) The thermal impedance and (f) λ_{eff} versus pressure for different composites.

pation process of the cooling system, which consisted of a CPU and an aluminum heat sink, as shown in Fig. 1(b). Table 2 shows the relevant parameters of the composites used in the simulation. The temperature evolution on the data line (the yellow line in Fig. 2b) at the center of the model was recorded, and the maximum temperature of CPU was recorded every 4 s.

Fig. 8(a) shows the heat transfer process of different CPU systems. Because of pure SR has very low thermal conductivity and high contact resistance, the heat transfer from the CPU is quite slow. The heat transfer is significantly enhanced due to the increase in the thermal conductivity and decrease in the contact resistance with the addition of h-BN content. However, the increase in BLT and contact resistance as h-BN content further increases, leading to difficulties in improving heat transfer effectively. Concretely, the CPU temperature in the case of pure SR as TIMs rises to about 93.4 °C within 300 s and then gradually rises to 96.8 °C within 600 s (Fig. 8b). When the content of h-BN reaches 90 phr, the maximum temperature of CPU drops sharply to 65.7 °C. However, the maximum temperature of CPU only decreases by about 3 °C when the h-BN content further increases from 90 phr to 180 phr,

https://doi.org/10.1007/s10118-023-3023-2

which is consistent with the thermal impedance results (Fig. 7d). In addition, the temperature gradient from the CPU to the heat sink decreases with increasing the content of the h-BN as shown in Fig. 8(c). These results indicate that high thermal conductivity in the TIMs does not mean efficient heat dissipation since the contact resistance and BLT are also components of the thermal impedance.

Discussion on the Thermal Impedance of the Composites

To obtain an in-depth understanding of the effect of h-BN on the thermal impedance of SR composites, the surface morphology of the composites was characterized by SEM and 3D profiler. SR composites exhibit a relatively smooth and dense surface at low h-BN content, shown in Fig. 9(a). Small defects begin to appear and the h-BN is exposed on the surface of the composites with the increase of h-BN, leading to the reduced filling capacity of air gaps. When the composites are placed between the processor and the heat sink, it is likely to lead to an increase in contact resistance due to the restricted actual contact area. 3D contour images (Fig. 10) demonstrate that the surface roughness averages (Sa) of the composites increases with increasing h-BN content. Based on the SEM and 3D contour images, it can be known that the introduction of h-BN has led to a deterioration in conformity of the composites.

The thermal impedance of TIMs is given by Eq. (2), which depends on λ, contact resistance and BLT. As shown in Table 1, pure SR has a quite low elastic modulus (about 0.90 MPa) and is highly susceptible to the deformation under the assembly pressure. The excessive compression deformation of the pure SR at 0.69 MPa warps the contact surfaces and reduces the actual contact area, resulting in high contact resistance (Fig. 11a). The elastic modulus increases and the ability to withstand deformation improves with increasing the h-BN content, which is manifested by a gradual increase in the BLT. Simultaneously, the conformity of the composites decreased with increasing the h-BN content. SR90 shows sufficient conformity due to its appropriate elastic modulus and relatively low Sa at the assembly pressure of 0.69 MPa, resulting in the

Table 2 Parameters used in the simulation.

Sample	BLT (mm)	Contact resistance ($K \cdot cm^2 \cdot W^{-1}$)	Specific heat ($J \cdot g^{-1} \cdot °C^{-1}$)	Density (g/cm^3)	Thermal conductivity ($W \cdot m^{-1} \cdot K^{-1}$)	
					Through-plane	In-plane
SR	1.28	12.89	1.034	0.97	0.20	0.20
SR60	1.54	3.52	0.987	1.24	0.49	1.81
SR90	1.62	0.39	0.980	1.33	0.65	2.89
SR120	1.71	1.03	0.891	1.41	0.75	4.09
SR180	1.95	1.43	0.885	1.54	1.01	7.04

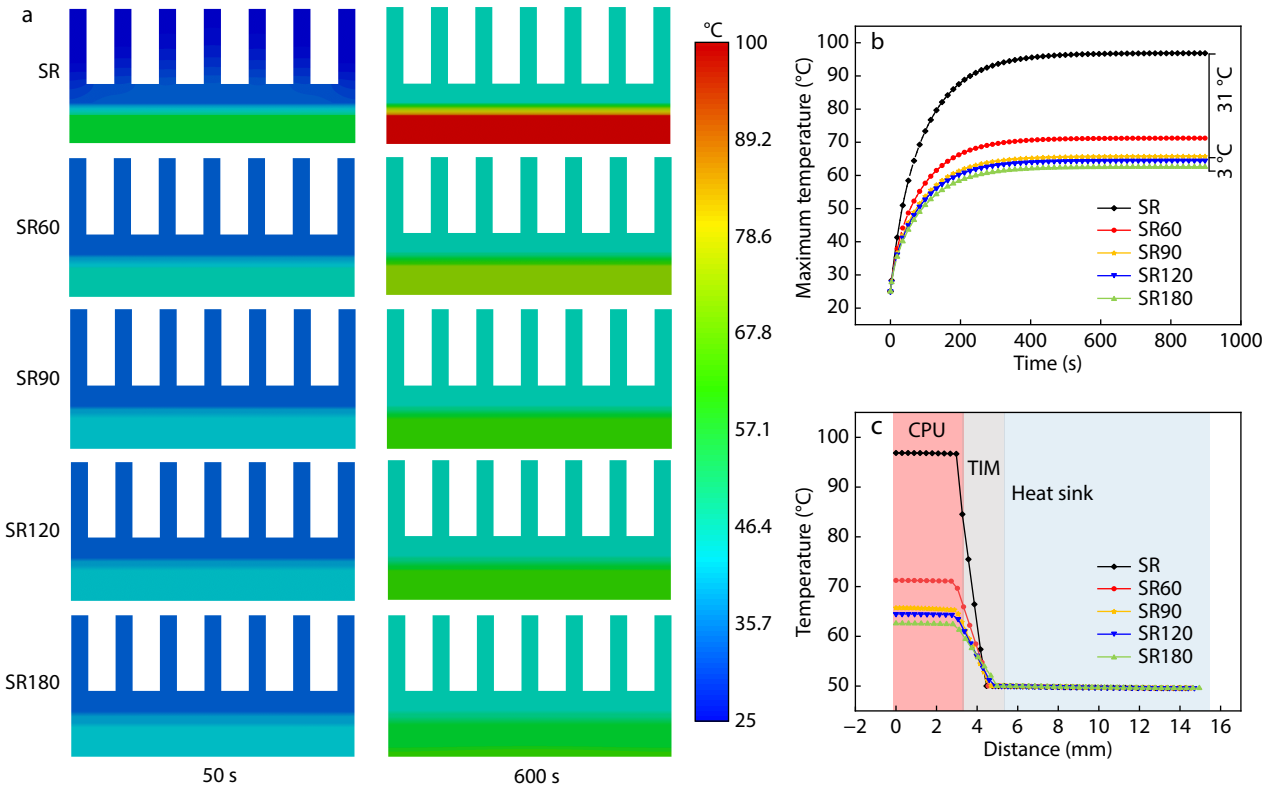

Fig. 8 (a) Heat transfer process of different CPU systems by finite element analysis (b) The maximum temperature of CPU versus time; (c) Variation of CPU system temperature along the data line.

https://doi.org/10.1007/s10118-023-3023-2

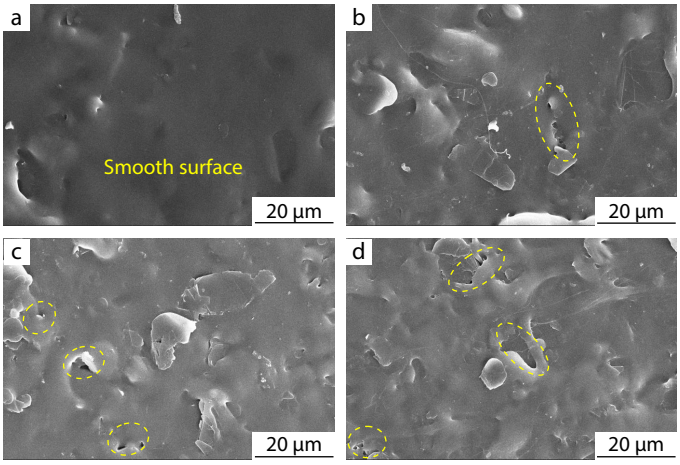

Fig. 9 SEM images of the composites surface: (a) SR60, (b) SR90, (c) SR120, (d) SR180.

lowest contact thermal resistance (Fig. 11b). However, as the h-BN content further increases, the high elastic modulus and Sa of the composites prevents it from replacing the air-filled voids and instead leads to a deterioration of the contact resistance (Fig. 11c). Furthermore, the through-plane thermal conductivity increases slowly with the increase of the h-BN content, due to the dense stacking and in-plane orientation of the h-BN. Taking λ, contact resistance and BLT into account, the decrease in thermal impedance of the SR composites is non-linear, as shown in Fig. 7(a). Consequently, the performance of the SR composites as TIMs can be evaluated more precisely by the thermal impedance.

In addition to the characteristics of the SR composites as TIMs, the assembly pressure is also a key factor to be considered. TIMs need close contact at the interfaces to fill voids and reduce contact resistance. The λ_{eff}, which is obtained from the ratio of BLT to θ, represents the overall effectiveness of the TIMs. As shown in Fig. 7(f), the λ_{eff} of the composites always rises first and then falls with increasing the assembly pressure. Such tendency mainly derives from the mechanical response to the assembly pressure. In the beginning, the increase of the pressure not only promotes the interfacial heat transfer but also decreases the BLT, resulting in a significant enhancement of λ_{eff}. However, the warpage of the contact surfaces leads to the increase in the contact resistance, which is similar to the fact that pure SR has an extremely high contact re-

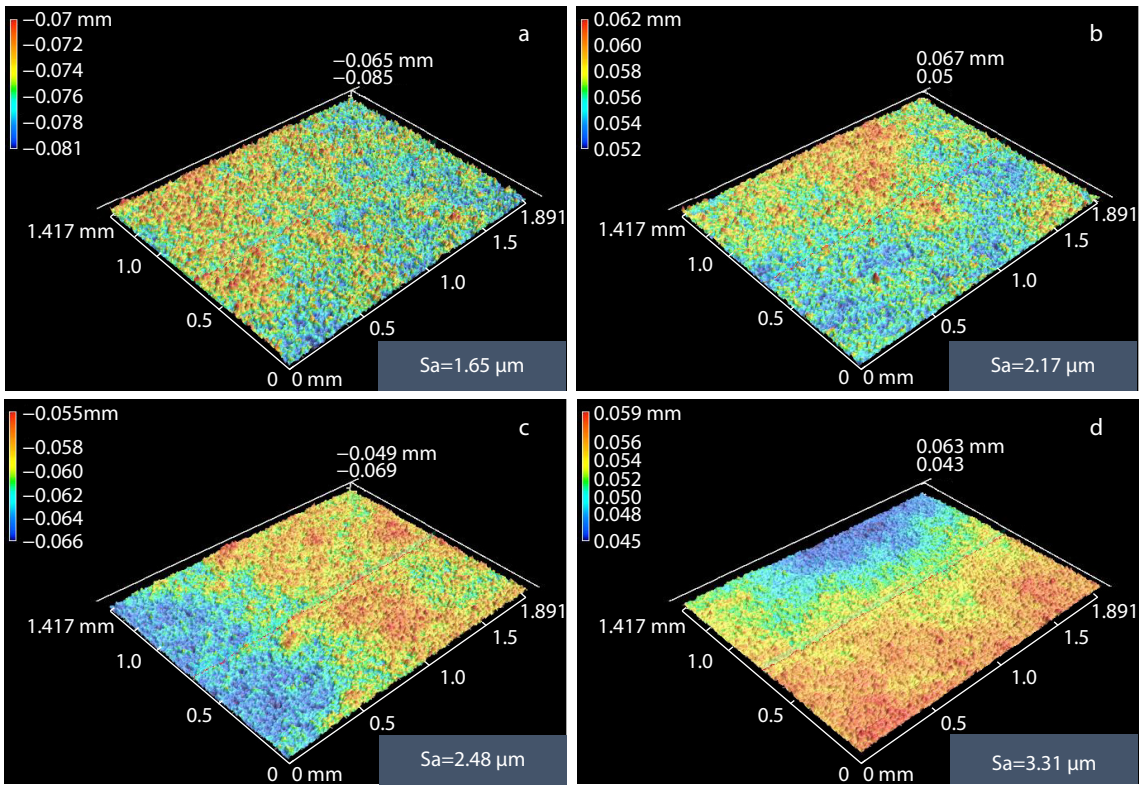

Fig. 10 3D contour images of the composites: (a) SR60, (b) SR90, (c) SR120, (d) SR180.

https://doi.org/10.1007/s10118-023-3023-2

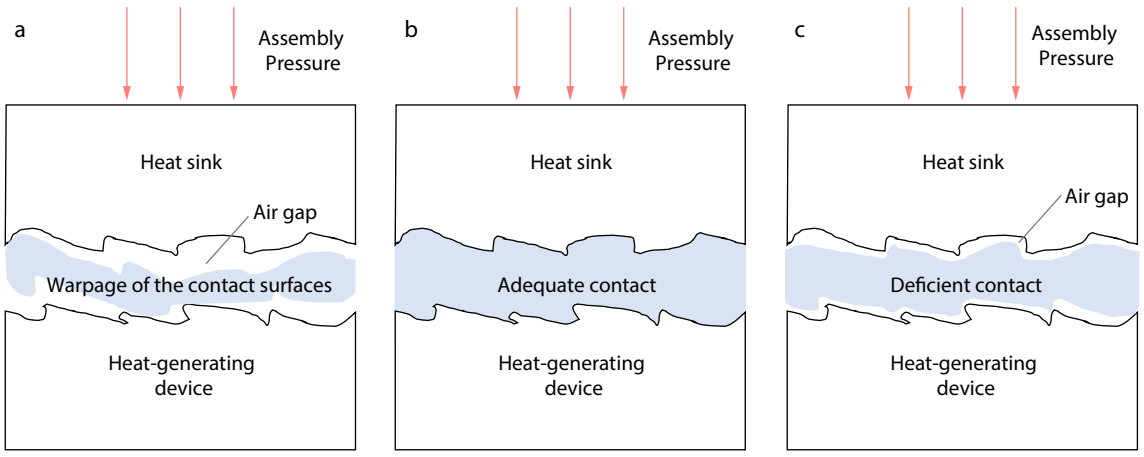

Fig. 11 Schematic representation of contact between heat sink and heat-generating device: (a) warpage of the contact surfaces, (b) adequate contact, (c) deficient contact.

sistance at a pressure of 0.69 MPa. Therefore, it is necessary to adjust the assembly pressure according to the compression properties of the TIMs, to achieve the highest λ_{eff}. Simultaneously, controlling BLT at a lower level is favorable to further improve the overall effectiveness of the TIMs according to Fig. 1(a).

CONCLUSIONS

In summary, the thermal conductivity, mechanical properties and thermal impedance of SR composites loaded with different levels of h-BN as TIMs were deeply investigated. The dense stacking and in-plane orientation of h-BN was confirmed by SEM, XRD and rheological analysis, resulting in a significant enhancement in in-plane thermal conductivity with increasing the h-BN content. The ASTM D 5470 standard test and finite element simulation results revealed that the thermal impedance of SR composites as TIMs was not only dependent on the thermal conductivity but also the contact resistance and BLT. Meanwhile, the contact resistance was influenced by the h-BN content. When the loading of h-BN was 90 phr, the contact resistance reached a minimum value of 0.39 $K{\cdot}cm^2{\cdot}W^{-1}$ at an assembly pressure of 0.69 MPa. Besides, the BLT decreased with increasing the assembly pressure, which should be adjusted to avoid the warpage of the contact surfaces and the increase in contact resistance according to the compression properties of SR composites. The understanding of the thermal impedance of SR composites as TIMs is versatile and can be readily extended to evaluate other polymer-based TIMs, which provides a significant guide to the design of high-performance TIMs.

Conflict of Interests

The authors declare no interest conflict.

ACKNOWLEDGMENTS

This work was financially supported by Sichuan Science and Technology Program (No. 2022YFH0090) and the Fundamental Research Funds for the Central Universities.

REFERENCES

1 Razeeb, K. M.; Dalton, E.; Cross, G. L. W.; Robinson, A. J. Present and future thermal interface materials for electronic devices. *Int. Mater. Rev.* **2018**, *63*, 1–21.
2 Swamy, M. C. K.; Satyanarayan. A review of the performance and characterization of conventional and promising thermal interface materials for electronic package applications. *J. Electron. Mater.* **2019**, *48*, 7623–7634.
3 Zhao, Y.; Zeng, X.; Ren, L.; Xia, X.; Zeng, X.; Zhou, J. Heat conduction of electrons and phonons in thermal interface materials. *Mater. Chem. Front.* **2021**, *5*, 5617–5638.
4 Li, J.; Liu, X.; Feng, Y.; Yin, J. Recent progress in polymer/two-dimensional nanosheets composites with novel performances. *Prog. Polym. Sci.* **2022**, *126*, 101505.
5 Huang, T.; Yang, F.; Wang, T.; Wang, J.; Li, Y.; Huang, J.; Chen, M.; Wu, L. Ladder-structured boron nitride nanosheet skeleton in flexible polymer films for superior thermal conductivity. *Appl. Mater. Today* **2022**, *26*, 101299.
6 Niu, H.; Guo, H.; Ren, Y.; Ren, L.; Lv, R.; Kang, L.; Bashir, A.; Bai, S. Spherical aggregated BN /AlN filled silicone composites with enhanced through-plane thermal conductivity assisted by vortex flow. *Chem. Eng. J.* **2022**, *430*, 133155.
7 Zhao, N.; Li, J.; Wang, W.; Gao, W.; Bai, H. Isotropically ultrahigh thermal conductive polymer composites by assembling anisotropic boron nitride nanosheets into a biaxially oriented network. *ACS Nano* **2022**, *16*, 18959–18967.
8 Song, H.; Liu, J.; Liu, B.; Wu, J.; Cheng, H. M.; Kang, F. Two-dimensional materials for thermal management applications. *Joule* **2018**, *2*, 442–463.
9 Chaudhry, A. U.; Mabrouk, A. N.; Abdala, A. Thermally enhanced polyolefin composites: fundamentals, progress, challenges, and prospects. *Sci. Technol. Adv. Mater.* **2020**, *21*, 737–766.
10 Zhang, R.; Liu, Z.; Sun, Z.; He, X.; Lin, Q.; Xiang, Y.; Fang, X.; Li, S.; Fu, X.; Liu, Q.; Hu, S.; Ping Wong, C. A scalable highly thermal conductive silicone rubber composite with orientated graphite by pre-vulcanizing and multilayer stacking method. *Compos. Part A: Appl. Sci. Manuf.* **2022**, *157*, 106944.
11 Hu, Q.; Bai, X.; Zhang, C.; Zeng, X.; Huang, Z.; Li, J.; Li, J.; Zhang, Y. Oriented BN/silicone rubber composite thermal interface materials with high out-of-plane thermal conductivity and flexibility. *Compos. Part A: Appl. Sci. Manuf.* **2022**, *152*, 106681.
12 Yin, Z.; Guo, J.; Jiang, X. Significantly improved thermal conductivity of silicone rubber and aligned boron nitride composites by a novel roll-cutting processing method. *Compos.*

Sci. Technol. **2021**, *209*, 108794.
13 Feng, C. P.; Wan, S. S.; Wu, W. C.; Bai, L.; Bao, R. Y.; Liu, Z. Y.; Yang, M. B.; Chen, J.; Yang, W. Electrically insulating, layer structured SiR/GNPs/BN thermal management materials with enhanced thermal conductivity and breakdown voltage. *Compos. Sci. Technol.* **2018**, *167*, 456–462.
14 Xue, Y.; Li, X.; Wang, H.; Zhao, F.; Zhang, D.; Chen, Y. Improvement in thermal conductivity of through-plane aligned boron nitride/silicone rubber composites. *Mater. Des.* **2019**, *165*, 107580.
15 Zhou, W. Y.; Qi, S. H.; Zhao, H. Z.; Liu, N. L. Thermally conductive silicone rubber reinforced with boron nitride particle. *Polym. Compos.* **2007**, *28*, 23–28.
16 Kong, S. M.; Mariatti, M.; Busfield, J. J. C. Effects of types of fillers and filler loading on the properties of silicone rubber composites. *J. Reinf. Plast. Compos.* **2011**, *30*, 1087–1096.
17 Li, S. J.; Li, J. C.; Ji, P. Z.; Zhang, W. F.; Lu, Y. L.; Zhang, L. Q. Bubble-templated construction of three-dimensional ceramic network for enhanced thermal conductivity of silicone rubber composites. *Chinese J. Polym. Sci.* **2021**, *39*, 789–795.
18 Zhang, J.; Li, C.; Yu, C.; Wang, X.; Li, Q.; Lu, H.; Zhang, Q.; Zhao, J.; Songfeng, E.; Hu, M.; Yao, Y. Large improvement of thermal transport and mechanical performance of polyvinyl alcohol composites based on interface enhanced by SiO_2 nanoparticle-modified-hexagonal boron nitride. *Compos. Sci. Technol.* **2019**, *169*, 167–175.
19 Zhao, C.; Li, Y.; Liu, Y.; Xie, H.; Yu, W. A critical review of the preparation strategies of thermally conductive and electrically insulating polymeric materials and their applications in heat dissipation of electronic devices. *Adv. Compos. Hybrid Mater.* **2022**, *6*, 27.
20 Chen, Y.; Zhang, H.; Chen, J.; Guo, Y.; Jiang, P.; Gao, F.; Bao, H.; Huang, X. Thermally conductive but electrically insulating polybenzazole nanofiber/boron nitride nanosheets nanocomposite paper for heat dissipation of 5G base stations and transformers. *ACS Nano* **2022**, *16*, 14323–14333.
21 Guerra, V.; Wan, C.; McNally, T. Thermal conductivity of 2D nano-structured boron nitride (BN) and its composites with polymers. *Prog. Mater. Sci.* **2019**, *100*, 170–186.
22 Rasul, M. G.; Kiziltas, A.; Arfaei, B.; Shahbazian-Yassar, R. 2D boron nitride nanosheets for polymer composite materials. *npj 2D Mater. Appl.* **2021**, *5*, 56.
23 Weng, Q.; Wang, X.; Wang, X.; Bando, Y.; Golberg, D. Functionalized hexagonal boron nitride nanomaterials: emerging properties and applications. *Chem. Soc. Rev.* **2016**, *45*, 3989–4012.
24 Yu, S.; Shen, X.; Kim, J. K. Beyond homogeneous dispersion: oriented conductive fillers for high kappa nanocomposites. *Mater. Horiz.* **2021**, *8*, 3009–3042.
25 Khanum, K. K.; Jayaram, S. H. Improved thermal properties and erosion resistance of silicone composites with hexagonal boron nitride. *IEEE Trans. Ind. Appl.* **2022**, *58*, 6583–6590.
26 Qu, J.; Fan, L.; Mukerabigwi, J. F.; Liu, C.; Cao, Y. A silicon rubber composite with enhanced thermal conductivity and mechanical properties based on nanodiamond and boron nitride fillers. *Polym. Compos.* **2021**, *42*, 4390–4396.
27 Chen, Q.; Xi, B.; Zhang, J.; Yang, H.; Wang, X.; Chi, M. Dielectric properties and thermal conductivity of micro-BN-modified LSR used for high-voltage direct current cable accessories. *J. Mater. Sci.: Mater. Electron.* **2020**, *31*, 16583–16591.
28 Gu, J.; Meng, X.; Tang, Y.; Li, Y.; Zhuang, Q.; Kong, J. Hexagonal boron nitride/polymethyl-vinyl siloxane rubber dielectric thermally conductive composites with ideal thermal stabilities. *Compos. Part A: Appl. Sci. Manuf.* **2017**, *92*, 27–32.
29 Kemaloglu, S.; Ozkoc, G.; Aytac, A. Properties of thermally conductive micro and nano size boron nitride reinforced silicon rubber composites. *Thermochim. Acta* **2010**, *499*, 40–47.
30 Li, Y. T.; Liu, W. J.; Shen, F. X.; Zhang, G. D.; Gong, L. X.; Zhao, L.; Song, P.; Gao, J. F.; Tang, L. C. PProcessing, thermal conductivity and flame retardant properties of silicone rubber filled with different geometries of thermally conductive fillers: a comparative studyP. *Compos. Part B: Eng.* **2022**, *238*, 109907.
31 Liu, P.; Li, L.; Wang, L.; Huang, T.; Yao, Y.; Xu, W. Effects of 2D boron nitride (BN) nanoplates filler on the thermal, electrical, mechanical and dielectric properties of high temperature vulcanized silicone rubber for composite insulators. *J. Alloys Compd.* **2019**, *774*, 396–404.
32 Zhang, P.; Yuan, P.; Jiang, X.; Zhai, S.; Zeng, J.; Xian, Y.; Qin, H.; Yang, D. A theoretical review on interfacial thermal transport at the nanoscale. *Small* **2018**, *14*, 1702769.
33 Chung, D. D. L. Performance of thermal interface materials. *Small* **2022**, *18*, 2200693.
34 Zhao, D.; Qian, X.; Gu, X.; Jajja, S. A.; Yang, R. Measurement techniques for thermal conductivity and interfacial thermal conductance of bulk and thin film materials. *J. Electron. Packag.* **2016**, *138*, 040802.
35 Grujicic, M.; Zhao, C. L.; Dusel, E. C. The effect of thermal contact resistance on heat management in the electronic packaging. *Appl. Surf. Sci.* **2005**, *246*, 290–302.
36 Due, J.; Robinson, A. J. Reliability of thermal interface materials: a review. *Appl. Therm. Eng.* **2013**, *50*, 455–463.
37 Leong, C.-K.; Chung, D. D. L. Carbon black dispersions as thermal pastes that surpass solder in providing high thermal contact conductance. *Carbon* **2003**, *41*, 2459–2469.
38 Hu, K.; Chung, D. D. L. Flexible graphite modified by carbon black paste for use as a thermal interface material. *Carbon* **2011**, *49*, 1075–1086.
39 Goel, N.; Anoop, T. K.; Bhattacharya, A.; Cervantes, J. A.; Mongia, R. K.; Machiroutu, S. V.; Lin, H. L.; Huang, Y. C.; Fan, K. C.; Denq, B. L.; Liu, C. H.; Lin, C. H.; Tien, C. W.; Pan, J. H. Technical review of characterization methods for thermal interface materials (Tim). *2008 11th Intersociety Conference on Thermal and Thermomecha Phenomena in Electronic Systems* **2008**, 248–258.
40 Chen, J.; Huang, X.; Sun, B.; Wang, Y.; Zhu, Y.; Jiang, P. Vertically aligned and interconnected boron nitride nanosheets for advanced flexible nanocomposite thermal interface materials. *ACS Appl. Mater. Interfaces* **2017**, *9*, 30909–30917.
41 Du, X.; Yang, W.; Zhu, J.; Fu, L.; Li, D.; Zhou, L. Aligning diamond particles inside BN honeycomb for significantly improving thermal conductivity of epoxy composite. *Compos. Sci. Technol.* **2022**, *222*, 109370.
42 Zhu, Z.; Li, C.; Songfeng, E.; Xie, L.; Geng, R.; Lin, C. T.; Li, L.; Yao, Y. Enhanced thermal conductivity of polyurethane composites via engineering small/large sizes interconnected boron nitride nanosheets. *Compos. Sci. Technol.* **2019**, *170*, 93–100.
43 Li, Z.; Ju, D.; Han, L.; Dong, L. Formation of more efficient thermally conductive pathways due to the synergistic effect of boron nitride and alumina in poly(3-hydroxylbutyrate). *Thermochim. Acta* **2017**, *652*, 9–16.
44 Tanimoto, M.; Yamagata, T.; Miyata, K.; Ando, S. Anisotropic thermal diffusivity of hexagonal boron nitride-filled polyimide films: effects of filler particle size, aggregation, orientation, and polymer chain rigidity. *ACS Appl. Mater. Interfaces* **2013**, *5*, 4374–4382.
45 Zhang, X.; Zhang, J.; Xia, L.; Li, C.; Wang, J.; Xu, F.; Zhang, X.; Wu, H.; Guo, S. Simple and consecutive melt extrusion method to fabricate thermally conductive composites with highly oriented boron nitrides. *ACS Appl. Mater. Interfaces* **2017**, *9*, 22977–22984.
46 Xie, Y.; Yu, Y.; Feng, Y.; Jiang, W.; Zhang, Z. Fabrication of stretchable nanocomposites with high energy density and low

loss from cross-linked PVDF filled with poly(dopamine) encapsulated $BaTiO_3$. *ACS Appl. Mater. Interfaces* **2017**, *9*, 2995–3005.
47 Zhang, F.; Feng, Y.; Qin, M.; Gao, L.; Li, Z.; Zhao, F.; Zhang, Z.; Lv, F.; Feng, W. Stress controllability in thermal and electrical conductivity of 3D elastic graphene-crosslinked carbon nanotube sponge/polyimide nanocomposite. *Adv. Funct. Mater.* **2019**, *29*, 1901383.
48 He, H.; Peng, W.; Liu, J.; Chan, X. Y.; Liu, S.; Lu, L.; Le Ferrand, H. Microstructured BN composites with internally designed high thermal conductivity paths for 3D electronic packaging. *Adv. Mater.* **2022**, *34*, e2205120.
49 Guo, H.; Niu, H.; Zhao, H.; Kang, L.; Ren, Y.; Lv, R.; Ren, L.; Maqbool, M.; Bashir, A.; Bai, S. Highly anisotropic thermal conductivity of three-dimensional printed boron nitride-filled thermoplastic polyurethane composites: effects of size, orientation, viscosity, and voids. *ACS Appl. Mater. Interfaces* **2022**, *14*, 14568–14578.
50 Prasher, R. S.; Shipley, J.; Prstic, S.; Koning, P.; Wang, J. L. Thermal resistance of particle laden polymeric thermal interface materials. *ASME. J. Heat Transfer.* **2003**, *125*, 1170–1177.

https://doi.org/10.1007/s10118-023-3023-2